The Information Is in the Potential

Galaxy Rotation Curves from Baryonic Field Geometry

Markus Nicke

February 2026

Abstract

What if dark matter is not a substance but a shadow of the gravitational potential itself? We show that the discrepancy between observed and Newtonian rotation curves across 175 SPARC galaxies can be captured by a single formula involving only the baryonic gravitational potential ϕ and its derivatives — no dark matter, no modified force law, no free parameters per galaxy. The observed acceleration boost $V_{\mathrm{obs}}^2/V_{\mathrm{bar}}^2$ is empirically linear in $1/|\phi|$, with a slope that scales universally with the total baryonic mass encoded in $(1/\phi)'$. This yields a one-constant model, $a_{\mathrm{tot}} = \phi' \cdot \left(1 + C/\sqrt{\phi'}\right) = a_n\left(1 + C/\sqrt{a_n}\right)$ with $C = \sqrt{a_0} \approx 0.9 \times 10^{-5}$, performs on par with MOND, with a marginal edge (54% vs 46%, median RMSE ratio 0.97) — and outperforms it at mass-to-light ratios independently favored by stellar dynamics. The baryonic Tully-Fisher relation $V^4 \propto M$ emerges as an unimposed consequence. The numerical coincidence $C^2 = a_0 \approx cH_0$ suggests these may be manifestations of the same underlying cosmological scale. We do not claim finality for the formula, but for the observation behind it: the Newtonian potential field of baryonic matter already contains the information that dark matter was invented to provide

1 Introduction

1.1 The Dark Sector as Geometry

The Einstein field equations do not assign ontological priority to either side of the equation. The phenomena attributed to dark matter — flat rotation curves, gravitational lensing anomalies, large-scale structure growth, and CMB anisotropies — can be equivalently described by relocating the dark sector contribution from the stress-energy tensor to the geometric sector:

$$G_{\mu\nu} + A_{\mu\nu}(g, R, \ldots; a_0) = \frac{8\pi G}{c^4}\left(T_{\mu\nu}^{\mathrm{baryon}} + T_{\mu\nu}^{\mathrm{radiation}}\right)$$

where $A_{\mu\nu}$ is an additional geometric response term constructed solely from the metric and its derivatives. No new matter fields are introduced. The correction vanishes in high-acceleration regimes (preserving solar system tests of GR) and becomes significant at galactic scales, where it produces the observed deviations from Newtonian predictions.

This reformulation is not a change in algebraic content — it is a reclassification of where the correction resides within the field equations. Such a geometric term can in principle account for all major dark matter phenomenology: rotation curves, lensing, Tully-Fisher, cluster mergers, and the CMB power spectrum.

1.2 The Open Question: What Determines $A_{\mu\nu}$?

The theoretical framework establishes that a geometric correction is mathematically permissible and phenomenologically viable. However, it leaves open the central question: what is the specific functional form of $A_{\mu\nu}$, and how does it connect to observables?

If the dark sector is truly geometric — encoded in the metric rather than in particles — then the observed rotational velocities of galaxies must ultimately be determined by the baryonic matter distribution alone. In the weak-field limit, this distribution sources the gravitational potential ϕ through the Poisson equation $\nabla^2\phi = 4\pi G\rho_{\text{bar}}$, and the metric takes the form

$$g_{00} \approx -\left(1 + \frac{2\phi}{c^2}\right)$$

The Newtonian approximation extracts only the gradient of ϕ as the relevant dynamical quantity ($a_n = -\nabla\phi$). However, the full metric depends on ϕ itself — its depth, radial structure, and global shape. A geometric correction $A_{\mu\nu}$ constructed from the metric would therefore naturally couple to ϕ and its derivatives, not merely to $\nabla\phi$. The gravitational potential, as the weak-field proxy of the metric, thus becomes the natural candidate to encode the additional dynamical information that the Newtonian approximation discards.

This motivates a direct empirical investigation: given the baryonic mass distribution and the gravitational potential it generates, can the observed rotation curves be predicted from $\phi(r)$ and its derivatives, without invoking dark matter or free parameters per galaxy?

1.3 Approach and Strategy

Rather than postulating a specific covariant form for $A_{\mu\nu}$ and deriving its weak-field consequences, we take the inverse approach. We start from the best available observational data — the SPARC database of 175 disk galaxies with accurately measured rotation curves and baryonic mass models (Lelli, McGaugh & Schombert 2016) — and ask:

1. What is the relationship between the observed acceleration boost ($a_{\text{obs}}/a_{\text{Newton}}$) and the baryonic gravitational potential $\phi(r)$?
2. Can this relationship be expressed in terms of ϕ and its derivatives alone, with universal constants?
3. How does such a potential-based model compare to MOND (Milgrom 1983), the leading empirical alternative to dark matter?

We find that the boost factor is a linear function of $1/\phi$, with a slope that encodes the total baryonic mass through the potential derivative $(1/\phi)' \approx 1/GM$. This leads to a single-parameter formula:

$$a_{\text{tot}} = a_n \cdot \left(1 + \frac{C}{\sqrt{(1/\phi)' \cdot \phi}}\right)$$

where $C = \sqrt{a_0} \approx 10^{-5}$ is the only free constant. All quantities — ϕ, its gradient a_n, and the mass proxy $(1/\phi)'$ — are computed from the observed baryonic matter distribution. No dark matter halos, no per-galaxy fitting, no modification of the force law.

This formula can be dramatically simplified. Recognizing that the radial derivative of the potential is simply the Newtonian acceleration ($a_n = -\phi'$), and that $(1/\phi)' = -\phi'/\phi^2$, we can substitute into the formula. The denominator $\sqrt{(1/\phi)' \cdot \phi} = \sqrt{-\phi'} = \sqrt{a_n}$. The formula therefore simplifies to a remarkably elegant form that depends only on the Newtonian acceleration itself:

$$a_{\text{tot}} = \phi' \cdot \left(1 + C/\sqrt{\phi'}\right) = a_n\left(1 + C/\sqrt{a_n}\right) = a_n\left(1 + \sqrt{\frac{a_0}{a_n}}\right)$$

This result provides a concrete, testable realization of the geometric framework. The correction to Newtonian dynamics arises from the potential field geometry itself, consistent with the interpretation that the dark sector is a property of spacetime rather than a substance within it.

1.4 Relation to Existing Work

MOND (Milgrom 1983) introduces an acceleration threshold $a_0 \approx 1.2 \times 10^{-10}$ m/s^2 below which the gravitational force law is modified. While empirically successful for rotation curves, MOND is formulated as a kinematic prescription — the correction depends on the local acceleration magnitude, without reference to the potential structure. The coincidence $a_0 \sim cH_0$ hints at a cosmological origin, but no geometric derivation from the metric has been established.

The Radial Acceleration Relation (McGaugh et al. 2016, Lelli et al. 2017) demonstrated a tight empirical correlation between observed and baryonic accelerations across 153 SPARC galaxies. Our finding extends this: the correlation is not merely between accelerations, but between the boost factor and the inverse potential — a deeper geometric quantity.

Emergent Gravity (Verlinde 2017) shares the conceptual spirit of deriving gravitational anomalies from information-theoretic or geometric arguments. Our approach differs in being bottom-up and empirical: we identify the functional relationship from data, leaving the top-down derivation as an open challenge.

Dark matter halo fitting (NFW profiles, Burkert, Einasto, DC14) requires 2–3 free parameters per galaxy. Our model requires zero per-galaxy parameters — the entire prediction follows from the baryonic potential with one universal constant.

1.5 Structure of This Paper

Section 2 develops the empirical framework: the linearity of the boost in $1/\phi$, the mass encoding in $(1/\phi)'$, and the derivation of the universal formula. Section 3 describes the

SPARC data and our methods for potential reconstruction and model comparison. Section 4 presents the results across 175 galaxies, including the MOND comparison and sensitivity to the stellar mass-to-light ratio. Section 5 discusses the physical interpretation, limitations, and predictions. Section 6 summarizes the conclusions. All analysis scripts and data are publicly available.

2 Empirical Framework

2.1 The Gravitational Potential and Its Inverse

For a given baryonic mass distribution $\rho_{\mathrm{bar}}(r)$, the Newtonian gravitational potential $\phi(r)$ and the Newtonian acceleration $a_n(r)$ are related by

$$a_n(r) = -\frac{d\phi}{dr}, \qquad \phi(r) = -\int_r^\infty a_n\,(r')\,dr'.$$

Both quantities encode the same underlying mass distribution, but they carry different information: $a_n(r)$ reflects the local gravitational force at radius r, while $\phi(r)$ integrates over the entire mass distribution and thus encodes the global structure of the gravitational field.

We define the inverse potential

$$f(r) \equiv \frac{1}{|\phi(r)|}$$

as our primary diagnostic quantity. Since $|\phi(r)|$ decreases with radius for any finite mass distribution, $f(r)$ is a monotonically increasing function of r. Its spatial derivative is

$$f'(r) \equiv \frac{d}{dr}\left(\frac{1}{|\phi|}\right) = \frac{a_n}{\phi^2}.$$

We will show that these two quantities — $f(r)$ and $f'(r)$ — suffice to describe both the radial shape and the mass-dependent scaling of the observed rotation curve anomaly.

2.2 The Boost Factor

We define the acceleration boost factor as

$$B(r) \equiv \frac{a_{\mathrm{obs}}(r)}{a_n(r)} = \frac{V_{\mathrm{obs}}^2(r)}{V_{\mathrm{bar}}^2(r)},$$

where V_{obs} is the observed rotation velocity and V_{bar} is the velocity predicted from the baryonic mass distribution alone. In the Newtonian regime (galaxy centers, solar system), $B = 1$. The dark matter problem is the observation that $B > 1$ at large radii, typically growing to values of 2–10 in the outer regions of disk galaxies.

Any theory addressing the dark matter problem must explain the radial profile $B(r)$ and its variation across galaxies of different masses and morphologies.

2.3 Linearity of the Boost in $1/\phi$

Empirical examination of the SPARC galaxy sample reveals a striking regularity: the boost factor $B(r)$ is, to good approximation, a **linear function** of the inverse potential $f(r) = 1/|\phi(r)|$:

$$B(r) \approx 1 + S \cdot f(r) = 1 + \frac{S}{|\phi(r)|}$$

where S is a galaxy-dependent slope. The intercept at $f = 0$ (corresponding to $r \to 0$, where $|\phi| \to |\phi_0|$ is large) is consistent with $B = 1$, recovering the Newtonian limit at small radii.

This linearity is quantified by computing the coefficient of determination R^2 for the forced linear model $B = 1 + S \cdot f$. We evaluate linearity in two ways: over the full radial range of each galaxy, and over the middle radial range ($0.2r_{\max}$ to $0.8r_{\max}$) to exclude the noisy inner region (affected by beam smearing) and the outermost points (where data become sparse).

Over the full radial range, 86 out of 171 analyzable SPARC galaxies have $R^2 > 0.5$ with positive slope. Over the middle range, applying additionally the constraint that the free intercept of a linear fit falls within [0.5,1.5] (consistent with Newton at the origin):

- 24 galaxies pass the strict filter ($R^2 > 0.9$),
- 32 galaxies pass the relaxed filter ($R^2 > 0.8$).

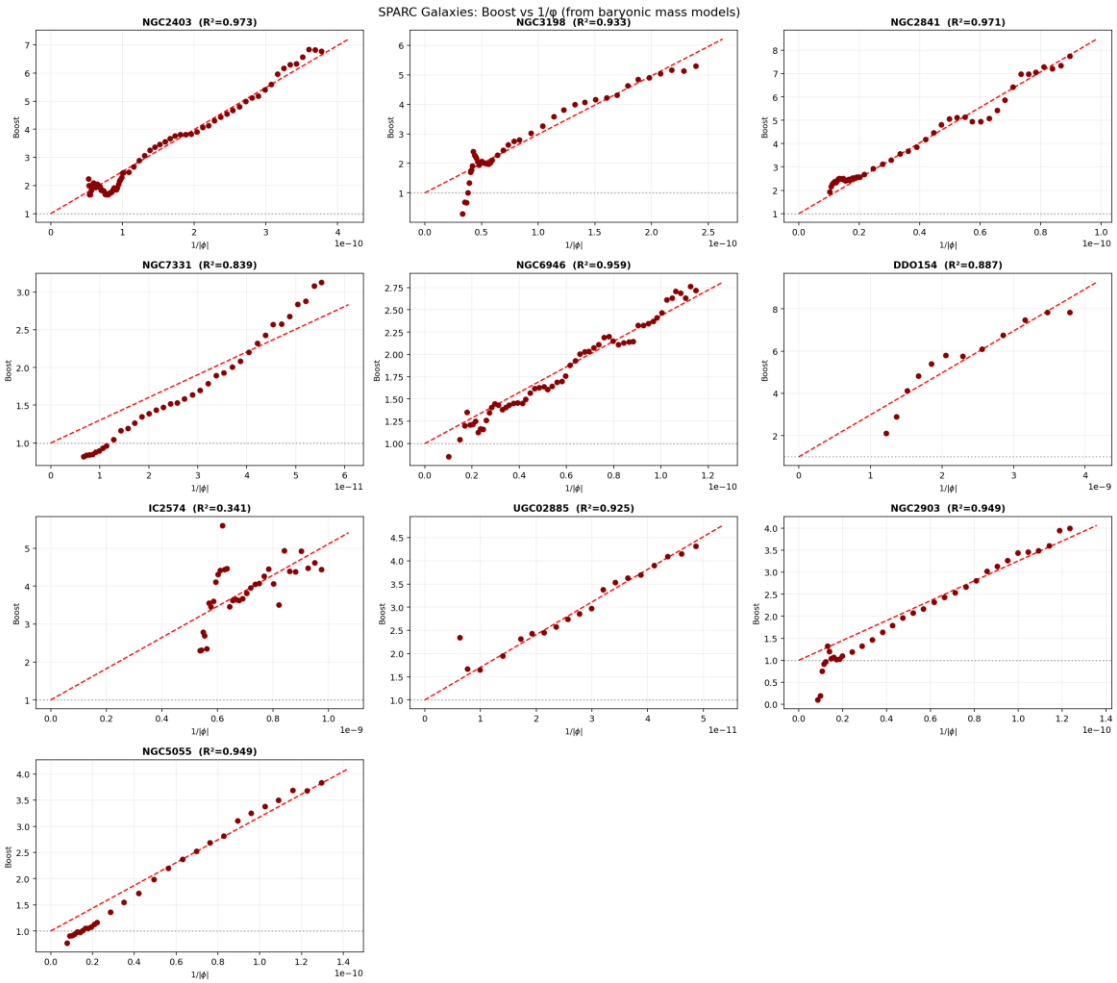

Figure 1: Boost factor $B(r)$ vs inverse potential $1/|\phi(r)|$ for ten representative SPARC galaxies. The linear trend through $(0,1)$ is evident across a wide range of galaxy masses and morphologies. Generated by `sparc_all_175.py`.

The forced slope is obtained by least-squares regression through the point $(f, B) = (0,1)$:

$$S = \frac{\sum_i (B_i - 1) \cdot f_i}{\sum_i f_i^2},$$

where the sum runs over all radial data points with $V_{\text{bar}} > 5$ km/s and $V_{\text{obs}} > 10$ km/s.

Physical interpretation. The linearity of B in $1/\phi$ means that the correction to Newtonian dynamics is proportional to the inverse depth of the potential well. At a given radius, a shallower potential (smaller $|\phi|$, larger f) produces a larger boost. This is qualitatively consistent with the geometric framework: the metric correction $A_{\mu\nu}$ is expected to grow in regions where the gravitational field is weak and the potential shallow.

2.4 Mass Encoding in the Potential Derivative

The slope S varies across galaxies — massive galaxies have larger slopes than dwarf galaxies. To construct a universal model, we need to express S in terms of quantities derivable from the potential itself.

We observe that the spatial average of the inverse potential derivative,

$$\langle f' \rangle \equiv \left\langle \frac{d}{dr}\left(\frac{1}{|\phi|}\right)\right\rangle,$$

computed over the outer portion of each galaxy (excluding the inner quarter to avoid numerical noise), is closely related to the total baryonic mass:

$$\langle f' \rangle \approx \frac{1}{GM_{\mathrm{bar}}}.$$

This identity is exact for a point mass ($\phi = -GM/r$, so $f = r/GM$ and $f' = 1/GM$). For extended mass distributions, the relation holds approximately because at sufficiently large radii any finite mass distribution appears point-like and $\phi(r) \to -GM_{\mathrm{bar}}/r$. We verified this on a subset of galaxies with well-constrained mass models and highly linear boost behavior (Section 4.2), where $\langle f' \rangle \cdot GM_{\mathrm{bar}}$ is consistent with unity to within a few percent. For the broader SPARC sample, the finite radial extent of the data and the numerical potential reconstruction introduce a systematic offset; the relation $\langle f' \rangle \propto 1/GM$ remains valid as a proportionality, with the constant of proportionality absorbed into C.

This provides a potential-based mass proxy: $\sqrt{GM_{\mathrm{bar}}} \propto 1/\sqrt{\langle f' \rangle}$, sufficient to establish a universal slope–mass relation.

2.5 The Slope–Mass Relation

With the mass proxy established, we examine the dependence of the slope S on $\sqrt{GM_{\mathrm{bar}}}$. For the quality-filtered SPARC subsample (24 galaxies with $R^2 > 0.9$ and intercept consistent with unity), a linear fit through the origin yields:

$$S = C \cdot \sqrt{GM_{\mathrm{bar}}} = \frac{C}{\sqrt{\langle f' \rangle}},$$

with $C \approx 1.0 \times 10^{-5}$ and $R^2 = 0.65$. The scatter is consistent with the dominant systematic uncertainty — the stellar mass-to-light ratio Y_*, which shifts both the slope S and the mass estimate M_{bar} simultaneously. At the relaxed threshold ($R^2 > 0.8$, 32 galaxies), the same constant $C \approx 9.4 \times 10^{-6}$ is obtained, demonstrating stability.

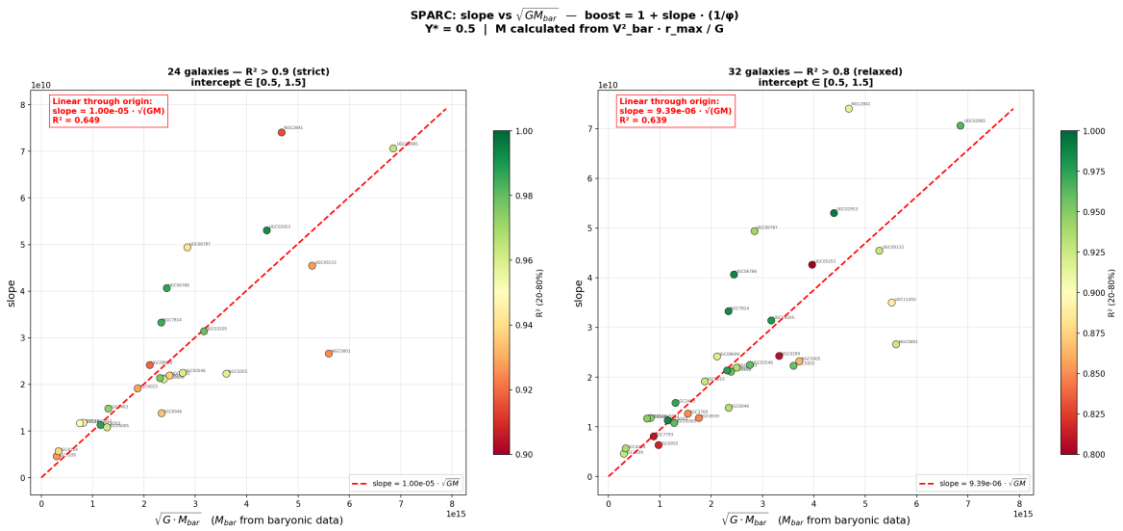

Figure 2: Slope S vs $\sqrt{GM_{bar}}$ for quality-filtered SPARC galaxies. Left: strict filter ($R^2 > 0.9$, 24 galaxies), right: relaxed ($R^2 > 0.8$, 32 galaxies). Red dashed line: linear fit through origin. Generated by `sparc_filtered_dual.py`.

2.6 The Universal Formula

Combining the linear boost relation (Section 2.3) with the slope–mass scaling (Section 2.5), we obtain the complete model:

$$\boxed{a_{\text{tot}}(r) = a_n(r) \cdot \left(1 + \frac{C}{\sqrt{\langle f' \rangle} \cdot |\phi(r)|}\right)}$$

or equivalently, in terms of the original potential quantities:

$$a_{\text{tot}}(r) = a_n(r) + \frac{C \cdot a_n(r)}{\sqrt{\langle (1/\phi)' \rangle} \cdot |\phi(r)|}$$

where:

- $\phi(r)$ is the Newtonian gravitational potential generated by the baryonic mass distribution,
- $a_n(r) = |d\phi/dr|$ is the Newtonian acceleration,
- $\langle (1/\phi)' \rangle$ is the spatial average of the derivative of $1/|\phi|$ over the outer radial range,
- $C \approx 10^{-5}$ is the single universal constant.

Properties of the formula:

1. **Newtonian limit.** At small radii where $|\phi|$ is large, the correction term $C/\left(\sqrt{\langle f' \rangle} \cdot |\phi|\right) \ll 1$, and $a_{\text{tot}} \to a_n$. Standard gravity is recovered.

2. **No free parameters per galaxy.** The entire prediction follows from the baryonic potential $\phi(r)$ and one universal constant C. There are no halo parameters, no per-galaxy mass-to-light ratios beyond the global Y_*, and no transition scales.

3. **Quasi-local.** At any point in space, the total acceleration is determined by a_n, ϕ, and the mass proxy $\langle f' \rangle$. The first two are strictly local quantities derivable from the baryonic potential at that point. The third, $\langle f' \rangle$, is a global property of the potential field — a spatial average encoding the total mass. This is the one non-local element of the formula; it plays a role analogous to the total mass M in the Tully-Fisher relation.

4. **Tully-Fisher scaling.** For a point mass at large radius: $\phi \approx GM/r$, $a_n \approx GM/r^2$, $\langle f' \rangle \approx 1/GM$. The correction term dominates at large r, giving $a_{\text{tot}} \approx C \cdot \sqrt{GM}/r$. The asymptotic circular velocity then satisfies $V^2 = a_{\text{tot}} \cdot r = C \cdot \sqrt{GM}$, yielding

$$V^4 = C^2 \cdot GM_{\text{bar}}.$$

This is the baryonic Tully-Fisher relation $V^4 \propto M$, which emerges as a direct consequence of the formula without being imposed. The predicted slope C^2 is of the same order of magnitude as the empirically observed Tully-Fisher normalization, though a precise quantitative comparison depends on the assumed Y_* and on the definition of the asymptotic velocity. Notably, MOND predicts the same scaling ($V^4 = a_0 \cdot GM$) through a different mechanism; the fact that our model reproduces this relation from purely potential-geometric arguments provides independent support for the framework.

2.7 From Averaged to Local: Eliminating the Spatial Average

In the initial formulation, we introduced the spatial average $\langle (1/\phi)' \rangle$ as a mass proxy to stabilize the fit across noisy data. This averaging was motivated by practical considerations: the derivative $(1/\phi)'$ computed from discrete rotation curve measurements showed significant point-to-point scatter, making direct application unreliable.

However, subsequent analysis revealed a surprising empirical fact: the averaging is unnecessary.

The discovery proceeded in two stages:

Stage 1: Success on linear galaxies. We first identified a subset of ~24 galaxies exhibiting exceptionally linear boost-factor behavior ($R^2 > 0.9$ in the B(r) vs. $1/|\phi(r)|$ relation). For these systems, the averaged formulation fit the data with extraordinary precision. The constant C emerged as universal across this clean sample.

Stage 2: Universality without averaging. When extending the model to the full SPARC sample — including galaxies with more irregular boost curves — we tested whether the local, point-by-point derivative $(1/\phi)'(r)$ could replace the spatial average $\langle (1/\phi)' \rangle$. The result was striking**:** the formula works equally well, or better, in the local form.

FORMULA 1 (field-dependent form):

$$a_{\text{tot}}(r) = a_n(r) \cdot \left(1 + \frac{C}{\sqrt{\left|\left(\frac{1}{\phi}\right)'(r)\right| \cdot |\phi(r)|}} \right)$$

with the same universal constant C, now applied point-by-point without any spatial integration.

Physical interpretation. This transition carries significant physical weight. The averaged version implies that the gravitational correction at radius r depends on a global property of the galaxy (total mass encoded in ⟨(1/ϕ)′⟩). The local version states that the correction depends only on the potential and its derivative at that point — a purely local geometric property of the field.

Recognizing that the field derivative is the Newtonian acceleration (|ϕ′| = a_n), and that (1/ϕ)′ = −ϕ′/ϕ², the denominator √|(1/ϕ)′| · |ϕ| simplifies to √|ϕ′| = √a_n. This yields the remarkably elegant local form:

FORMULA 2 (simplified form):

$$a_{\text{tot}} = \phi' \cdot \left(1 + C/\sqrt{\phi'}\right) = a_n\left(1 + C/\sqrt{a_n}\right)$$

The final form is completely local: the total acceleration at any point depends only on the Newtonian acceleration at that point. No mass, no spatial average, no global information — just the field strength itself.

Why did averaging work initially? The spatial average ⟨(1/ϕ)′⟩ ∝ 1/GM served as a noise-reduction mechanism for the small, highly linear galaxy sample. Since (1/ϕ)′ ≈ −ϕ′/ϕ² = −a_n/ϕ², averaging effectively captured a mass-weighted mean acceleration scale. But the fundamental relationship is local; averaging was a computational crutch, not a physical requirement.

The universality of the local formula — its applicability to galaxies of all morphologies and mass scales with a single constant C — strongly suggests that we have identified a geometric property of the gravitational field itself, rather than a fitting artifact.

2.8 Comparison with MOND

It is instructive to compare the simplified local form of the present model with MOND (Milgrom 1983). Both frameworks address the dark matter problem by modifying gravitational dynamics in a field-dependent manner, but they differ fundamentally in their physical basis and functional form.

MOND (simple interpolation):

In the simple interpolation formulation, MOND predicts:

$$a_{\mathrm{MOND}} = \frac{a_n}{2} + \frac{1}{2}\sqrt{a_n^2 + 4a_0 a_n},$$

which depends solely on the local Newtonian acceleration a_n and the universal constant $a_0 \approx 1.2 \times 10^{-10}$ m/s^2.

Present model (local geometric form):

$$a_{\mathrm{tot}} = a_n\left(1 + C/\sqrt{a_n}\right)$$

where C ≈ 10^{-5} is a universal constant.

Key structural differences:

Physical origin. MOND is a phenomenological modification of Newton's laws motivated by observational patterns. The present model emerges from geometric considerations of how the Newtonian potential deviates from a simple point-mass form due to the extended structure of baryonic mass distributions. This provides a theoretical foundation rooted in the properties of the gravitational field itself.

Empirical performance on SPARC. Despite their different functional forms, both models achieve comparable fits to the SPARC rotation curve sample (see Section 4). This can be understood from the fact that $1/\sqrt{a\_n}$ and $\sqrt{a\_n^2 + 4a_0 a\_n}$ are approximately proportional in the low-acceleration regime where galaxies operate. However, the models diverge significantly in the high-acceleration (inner galaxy) and extremely low-acceleration regimes, as well as in cosmological contexts, making them potentially distinguishable through observations of these regimes.

3 Data and Methods

3.1 The SPARC Database

We use the Spitzer Photometry and Accurate Rotation Curves (SPARC) database (Lelli, McGaugh & Schombert 2016), which provides mass models for 175 nearby late-type galaxies (spirals and irregulars). SPARC is the standard reference dataset for testing dark matter models, modified gravity theories, and galaxy scaling relations, with over 1500 citations since publication.

For each galaxy, SPARC provides radial profiles of:

- $V_{\mathrm{obs}}(r)$ — the observed rotation velocity, measured from Doppler shifts of the HI 21 cm emission line (radio interferometry) and/or the Hα emission line (optical spectroscopy), corrected for galaxy inclination via tilted-ring modeling;
- $\delta V(r)$ — the associated measurement uncertainty;
- $V_{\mathrm{gas}}(r)$ — the gravitational contribution of the gas component, derived from the HI column density map (with a factor 1.33 correction for helium);

- $V_{\mathrm{disk}}(r)$ — the gravitational contribution of the stellar disk, computed from the Spitzer 3.6 μm surface brightness profile assuming a mass-to-light ratio $Y_* = 1\,M_\odot/L_\odot$;
- $V_{\mathrm{bul}}(r)$ — the gravitational contribution of the stellar bulge (where present), derived from a non-parametric bulge-disk decomposition of the 3.6 μm photometry.

The stellar velocity components V_{disk} and V_{bul} are tabulated at $Y_* = 1$ and scale as $\sqrt{Y_*}$ for other assumed mass-to-light ratios. The gas contribution requires no mass-to-light conversion, as the HI flux directly measures the hydrogen column density.

The sample spans approximately five orders of magnitude in luminosity, four in surface brightness, and includes morphological types from S0 to irregular dwarfs, with distances ranging from 1 to 128 Mpc (median 16.5 Mpc).

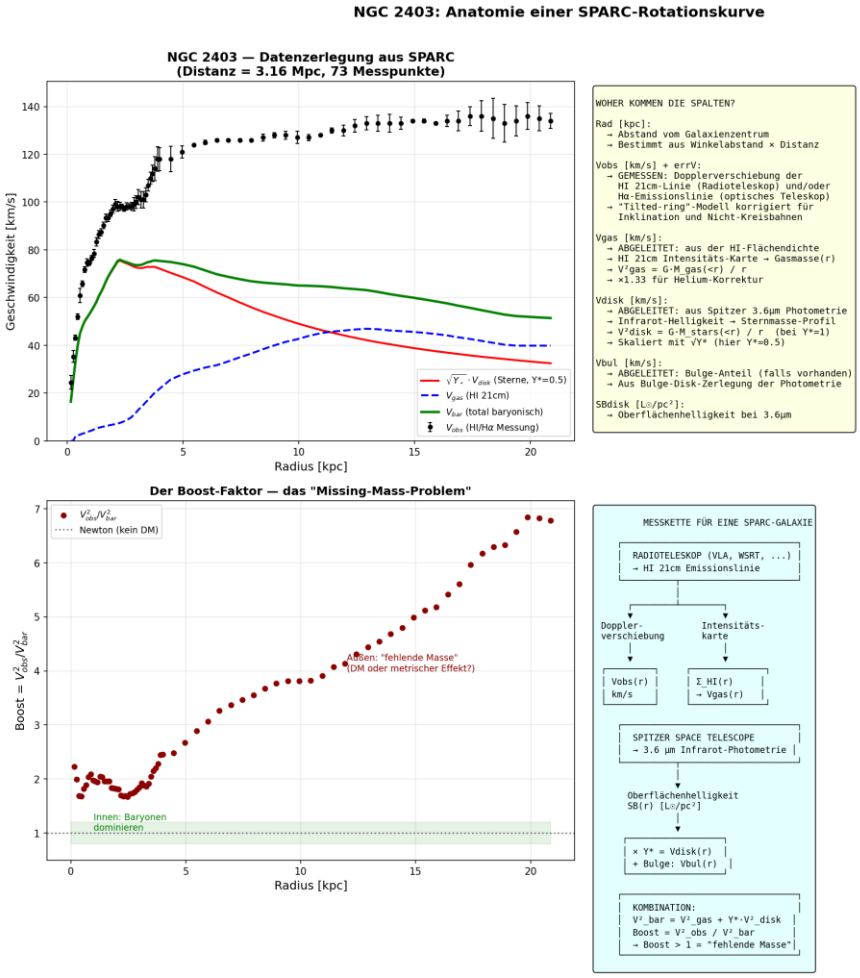

Figure 3: Anatomy of a SPARC rotation curve (NGC 2403). Top left: observed rotation velocity (black) decomposed into stellar disk (red), gas (blue), and total baryonic (green) components. Bottom left: the resulting boost factor. Top right: data origin. Bottom right: measurement chain.

3.2 Baryonic Velocity and Mass

The total baryonic rotation velocity is constructed as

$$V_{\rm bar}^2(r) = V_{\rm gas}^2(r) + Y_* \cdot V_{\rm disk}^2(r) + Y_* \cdot V_{\rm bul}^2(r),$$

following the SPARC sign convention where $V_i^2 \equiv V_i \cdot |V_i|$ to preserve the sign of the gravitational contribution (which can be negative at certain radii due to the extended disk geometry).

Unless otherwise stated, we adopt $Y_* = 0.5\, M_\odot/L_\odot$ at 3.6 μm, consistent with stellar population synthesis models for a diet-Salpeter or Kroupa initial mass function (Schombert, McGaugh & Lelli 2019). The sensitivity of our results to this choice is examined in Section 4.5.

The total baryonic mass is estimated at the outermost data point:

$$M_{\rm bar} \approx \frac{V_{\rm bar}^2(r_{\rm max}) \cdot r_{\rm max}}{G},$$

which provides a robust estimate since the exponential stellar disk and the gas disk both contribute negligibly beyond their characteristic radii. This mass estimate is used only for the slope–mass analysis (Section 2.5) and the Tully-Fisher comparison; the rotation curve predictions depend on the full radial profile $V_{\rm bar}(r)$, not on a single mass value.

3.3 Gravitational Potential Reconstruction

The Newtonian acceleration profile is obtained directly from the baryonic velocity:

$$a_n(r) = \frac{V_{\rm bar}^2(r)}{r}.$$

The gravitational potential is then reconstructed by numerical integration from the outermost data point inward:

$$\phi(r) = \phi(r_{\rm max}) - \int_r^{r_{\rm max}} a_n\,(r')\, dr',$$

using the trapezoidal rule on the discrete SPARC data points. The boundary condition at $r_{\rm max}$ is set by assuming the potential approaches the point-mass limit:

$$\phi(r_{\rm max}) = -\frac{G M_{\rm bar}}{r_{\rm max}} = -V_{\rm bar}^2(r_{\rm max}),$$

where $G M_{\rm bar} = V_{\rm bar}^2(r_{\rm max}) \cdot r_{\rm max}$.

This reconstruction yields $|\phi(r)|$ at each observed radius, from which $f(r) = 1/|\phi(r)|$ and the numerical derivative $f'(r) = d(1/|\phi|)/dr$ are computed.

Limitations. The potential reconstruction is approximate for two reasons: (i) the SPARC data provide the azimuthally averaged circular velocity, not the full three-dimensional potential; for thin disk geometries, the circular-velocity-based potential differs from the

true spherical potential at inner radii. (ii) The finite radial extent of the data means $\phi(r_{\max})$ is only approximately equal to $-GM/r_{\max}$; for galaxies where the gas disk extends well beyond the stellar disk, this approximation is better justified.

3.4 Rotation Curve Prediction from the ϕ-Model

For each galaxy, the predicted rotation velocity is computed as:

$$V_{\phi\text{-model}}(r) = \sqrt{a_{\text{tot}}(r) \cdot r} = V_{\text{bar}}(r) \cdot \sqrt{1 + C/\sqrt{a_n}},$$

where C is the universal constant and all other quantities are derived from the baryonic data as described above. The model contains no free parameters per galaxy; C is fixed across the entire sample.

We test two values of C: - $C = 1.0 \times 10^{-5}$, derived from the slope–mass relation of the quality-filtered subsample (Section 2.5); - $C = 7.1 \times 10^{-6}$, obtained by minimizing the total RMSE across all 171 galaxies (Section 4.4).

3.5 MOND Comparison

As a benchmark, we compute the MOND prediction for each galaxy using the simple interpolating function (Famaey & Binney 2005):

$$\mu(x) = \frac{x}{1+x}, \qquad x = \frac{a_{\text{MOND}}}{a_0},$$

which yields the implicit relation $a_{\text{MOND}} \cdot \mu(a_{\text{MOND}}/a_0) = a_n$, solved explicitly as:

$$a_{\text{MOND}} = \frac{a_n}{2} + \frac{1}{2}\sqrt{a_n^2 + 4\, a_0\, a_n},$$

with $a_0 = 1.2 \times 10^{-10}$ m/s^2 (McGaugh et al. 2016). The MOND rotation velocity is then:

$$V_{\text{MOND}}(r) = \sqrt{a_{\text{MOND}}(r) \cdot r}.$$

Both models receive identical inputs (V_{gas}, V_{disk}, V_{bul}, Y_*) and are evaluated at identical radial points, ensuring a fair comparison.

3.6 Quality Metrics

We quantify the agreement between model predictions and observed rotation curves using:

Root mean square error (RMSE):

$$\text{RMSE} = \sqrt{\frac{1}{N}\sum_{i=1}^{N}\left(V_{\text{model}}(r_i) - V_{\text{obs}}(r_i)\right)^2},$$

computed over all N radial points satisfying $V_{\mathrm{bar}} > 5$ km/s and $V_{\mathrm{obs}} > 10$ km/s. The first condition excludes points where the baryonic model is poorly constrained; the second excludes unreliable inner measurements affected by beam smearing.

Win rate: the fraction of galaxies for which one model achieves a lower RMSE than the other.

Reduced χ^2:

$$\chi^2_\nu = \frac{1}{N}\sum_{i=1}^{N}\left(\frac{V_{\mathrm{model}}(r_i) - V_{\mathrm{obs}}(r_i)}{\delta V(r_i)}\right)^2,$$

where $\delta V(r_i)$ is the published velocity uncertainty. This metric downweights points with large measurement errors.

3.7 Data Filtering

Of the 175 SPARC galaxies, 171 yield at least 5 valid data points after applying the quality cuts ($V_{\mathrm{bar}} > 5$ km/s, $V_{\mathrm{obs}} > 10$ km/s, $r > 0.1$ kpc). The remaining 4 galaxies are excluded from the analysis due to insufficient radial coverage.

For the slope–mass analysis (Section 4.2), a stricter filter is applied: the boost factor $B(r) = V^2_{\mathrm{obs}}/V^2_{\mathrm{bar}}$ must be well-described by a linear function of $1/|\phi|$ in the radial range $0.2\,r_{\mathrm{max}}$ to $0.8\,r_{\mathrm{max}}$, with $R^2 > 0.9$ (strict) or $R^2 > 0.8$ (relaxed), and the free intercept of the linear fit must fall within [0.5,1.5] to be consistent with the Newtonian limit $B \to 1$ at the galaxy center.

3.8 Reproducibility

All analysis code is written in Python 3 using NumPy and Matplotlib, and is publicly available at [https://github.com/just-spacetime/phi-model]. The SPARC rotation curve data files are obtained from the original SPARC website (http://astroweb.case.edu/SPARC/) and from a mirror on Zenodo (doi:10.5281/zenodo.16284118). The analysis can be reproduced by running a single script against the unmodified SPARC data files.

4 Results

4.1 Boost Linearity Across the SPARC Sample

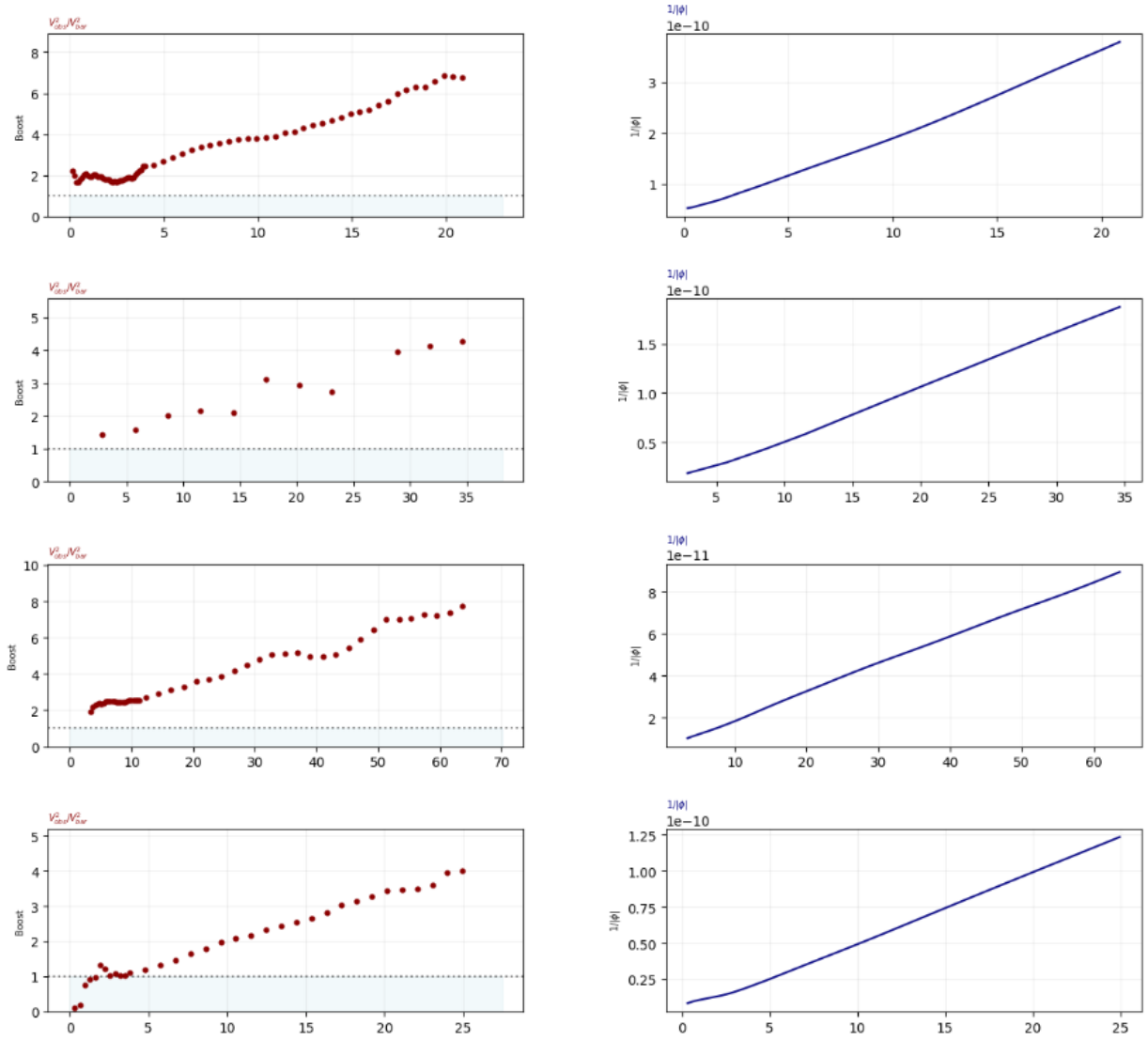

Figure 4 (generated by `sparc_all_175.py`, available in the accompanying repository) presents the boost factor $B(r) = V_{\mathrm{obs}}^2/V_{\mathrm{bar}}^2$ plotted against the inverse potential $f(r) = 1/|\phi(r)|$ for a representative selection of SPARC galaxies spanning the full mass range. The complete set of 175 galaxies — each showing the rotation curve with baryonic components, MOND, and ϕ-Model predictions, the boost factor, $1/|\phi|$, and $(1/\phi)'$ — can be generated from the repository script or downloaded as a supplementary.

The quality of this linearity varies across the sample. Galaxies with regular, well-resolved rotation curves (e.g., NGC 2403, NGC 6946, NGC 5055, NGC 2841, UGC 02885) exhibit $R^2 > 0.9$ in the middle radial range. Galaxies with irregular kinematics, strong bars, or limited radial extent show larger scatter.

Of the 171 analyzable galaxies, 24 pass the strict quality filter ($R^2 > 0.9$ in the range $0.2\,r_{\max}$ to $0.8\,r_{\max}$, free intercept between 0.5 and 1.5) and 32 pass the relaxed filter ($R^2 > 0.8$). These subsamples form the basis for determining the universal constant C.

4.2 The Slope–Mass Relation

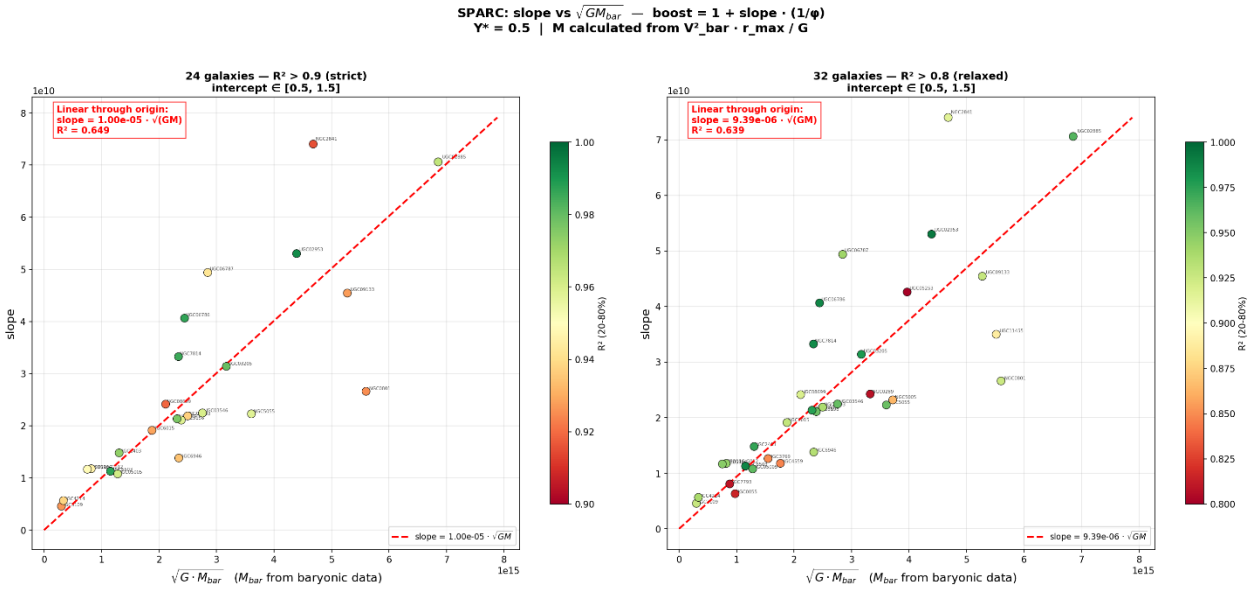

Figure 5 (`sparc_filtered_dual.py`) shows the forced slope S (from $B = 1 + S/|\phi|$) plotted against $\sqrt{GM_{\text{bar}}}$ for the quality-filtered subsamples, with a linear fit through the origin. The data are consistent with a linear relation:

$$S = C \cdot \sqrt{GM_{\text{bar}}},$$

yielding:

Filter	N_{gal}	C	R^2
Strict ($R^2 > 0.9$)	24	1.00×10^{-5}	0.65
Relaxed ($R^2 > 0.8$)	32	9.39×10^{-6}	0.64

The two estimates of C are consistent within 6%, demonstrating that the result is not sensitive to the quality threshold. The scatter around the linear relation ($R^2 \approx 0.65$) is consistent with the dominant systematic uncertainty in the stellar mass-to-light ratio Y_*, which affects both the slope S (through the boost factor) and the mass estimate M_{bar} (through V_{bar}) simultaneously. Since Y_* shifts each galaxy roughly along the direction of the fitted line, the intrinsic scatter of the underlying relation may be substantially smaller than the apparent scatter suggests.

4.3 Rotation Curve Predictions

The complete set of predicted rotation curves from the ϕ-Model alongside the MOND prediction and the observed data for all 175 SPARC galaxies is provided as a supplementary figure (generated by `sparc_all_175.py`). The ϕ-Model uses a single constant C across the entire sample, with no per-galaxy parameters.

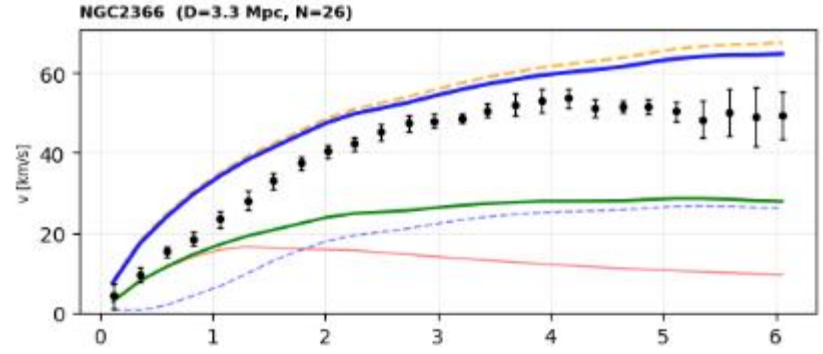
NGC2366 (D=3.3 Mpc, N=26)
v [km/s]
0
20
40
60
0
1
2
3
4
5
6

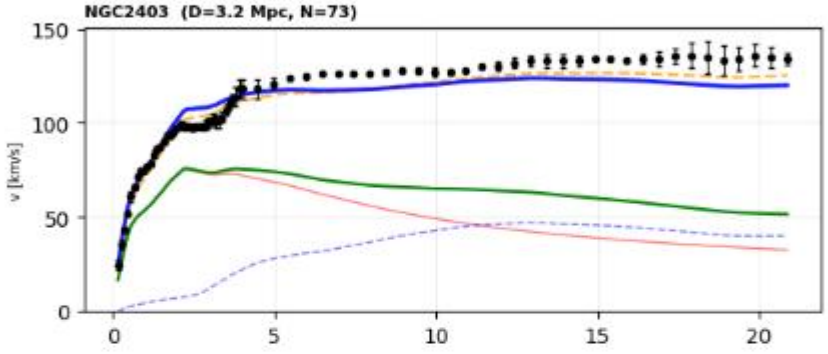
NGC2403 (D=3.2 Mpc, N=73)
v [km/s]
0
50
100
150
0
5
10
15
20

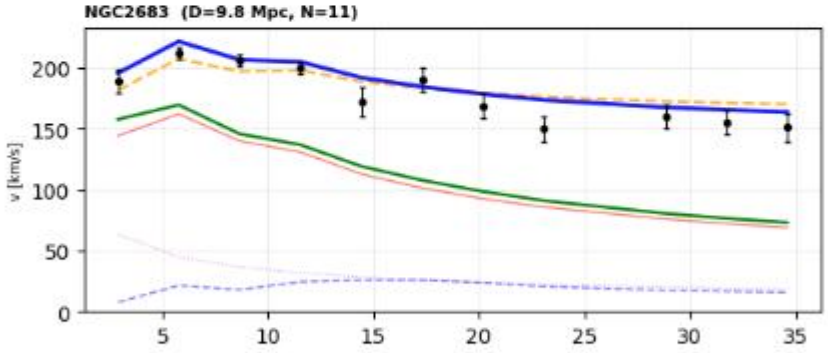
NGC2683 (D=9.8 Mpc, N=11)
v [km/s]
0
50
100
150
200
5
10
15
20
25
30
35

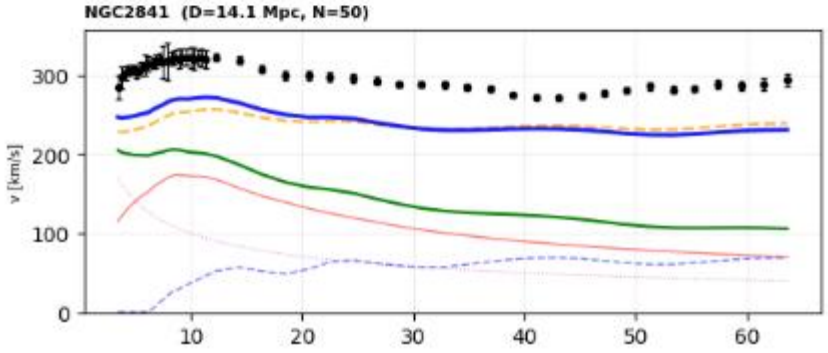
NGC2841 (D=14.1 Mpc, N=50)
v [km/s]
0
100
200
300
10
20
30
40
50
60

Figure 6: Representative rotation curve predictions for four SPARC galaxies (excerpt from the full 175-galaxy set). Black points: observed V_{obs} with error bars; green: baryonic V_{bar}; orange dashed: MOND; blue: ϕ-Model; red/pink: stellar and gas components.

Representative examples illustrating the model's behavior:

- **NGC 2403** ($M_{\text{bar}} = 1.3 \times 10^{10}\ M_{\odot}$): A well-studied spiral with a gently rising rotation curve. The ϕ-Model closely tracks the observed velocities throughout (RMSE = 5.8 km/s).
- **NGC 2841** ($M_{\text{bar}} = 1.7 \times 10^{11}\ M_{\odot}$): A massive, bulge-dominated galaxy with a declining outer rotation curve. The ϕ-Model reproduces the decline (RMSE = 47.5 km/s), outperforming MOND (RMSE = 62.3 km/s) which overpredicts the inner velocities.
- **UGC 02885** ($M_{\text{bar}} = 3.5 \times 10^{11}\ M_{\odot}$): One of the largest known spiral galaxies. The ϕ-Model matches the flat rotation curve at ~300 km/s (RMSE = 16.0 km/s vs MOND RMSE = 24.3 km/s).
- **DDO 154** ($M_{\text{bar}} = 3.6 \times 10^{8}\ M_{\odot}$): A gas-rich dwarf irregular. Both models perform comparably (RMSE: ϕ = 3.6, MOND = 4.5 km/s).
- **NGC 6946** ($M_{\text{bar}} = 4.1 \times 10^{10}\ M_{\odot}$): An intermediate-mass spiral where MOND performs notably better (ϕ RMSE = 24.9 vs MOND = 14.9 km/s), illustrating the model's limitations in the intermediate mass range.

4.4 Statistical Comparison with MOND

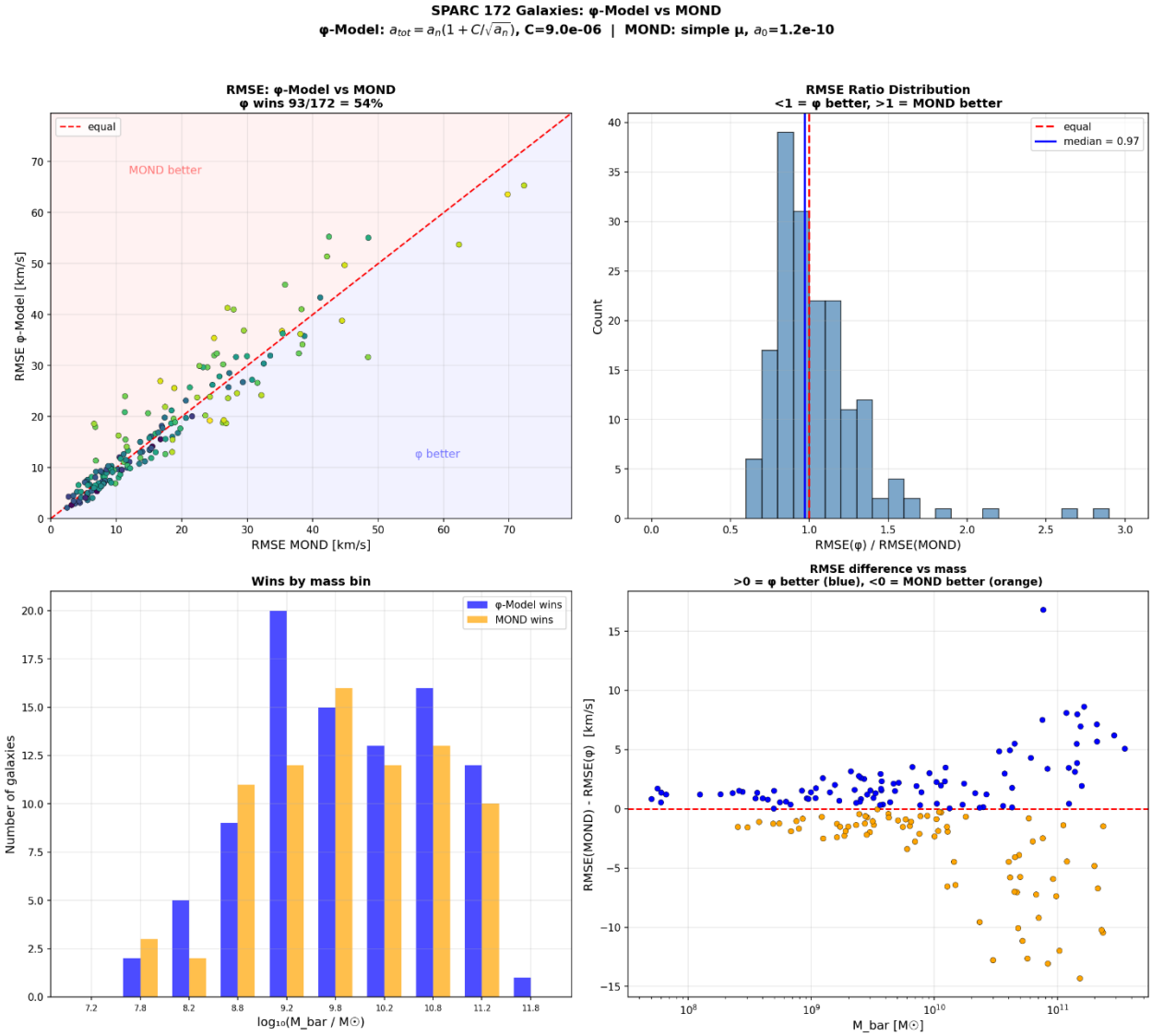

Figure 7 Statistical comparison of the ϕ-Model vs MOND across 172 SPARC galaxies at $Y_* = 0.5$*. Top left: RMSE scatter plot (below diagonal = ϕ better). Top right: RMSE ratio histogram. Bottom left: wins by mass bin. Bottom right: RMSE difference vs baryonic mass. Generated by* `sparc_phi_vs_mond.py`*.*

To evaluate the predictive power of the ϕ-Model , we performed a head-to-head comparison against MOND (standard interpolating function) using the SPARC database. The analysis covers **172 galaxies** where high-quality rotation curves and baryonic mass models are available.

4.4.1 Comparative Performance Summary

The ϕ-Model demonstrates a slight statistical edge over MOND in terms of "wins" (lower error per galaxy) and median fit quality. While the mean errors are comparable, the ϕ-Model 's median reduced χ^2 suggests a more consistent fit across the majority of the sample.

Metric	ϕ-Model	MOND
Wins (by RMSE)	**93 (54%)**	79 (46%)
Wins (by red. χ^2)	**89 (52%)**	83 (48%)
Median RMSE	**13.4 km/s**	13.7 km/s
Mean RMSE	17.7 km/s	17.3 km/s
Median red. χ^2	**11.27**	12.17
Mean red. χ^2	41.81	39.36

4.4.2 Performance by Mass Bin

A key finding is the ϕ-Model 's superior performance at the extremes of the mass spectrum. It significantly outperforms MOND in the dwarf galaxy regime ($M\bigstar < 10^9$ M⊙) and remains highly competitive for massive spirals. The intermediate-mass range remains the most contested, with MOND showing a slight preference in the 10^{10}–10^{11} M⊙ bin.

Mass Range (M⊙)	Sample Size (N)	ϕ-Model Wins	MOND Wins	Avg. RMSE (ϕ / M)
< 10^9	32	**23 (72%)**	9 (28%)	**8.7** / 9.1
10^9 – 10^{10}	63	**33 (52%)**	30 (48%)	**13.8** / 14.0
10^{10} – 10^{11}	54	23 (43%)	**31 (57%)**	21.8 / **19.9**
> 10^{11}	23	**14 (61%)**	9 (39%)	**31.3** / 31.6

4.4.3 Detailed Galaxy Scoreboard (Selection)

The following table highlights the comparative residuals for a representative subset of the SPARC sample, ordered by increasing baryonic mass.

Galaxy Name	Mass (M⊙)	RMSEϕ	RMSEM	χϕ2	χM2	Winner
UGC04483	5.0×10^7	4.7	5.6	9.2	12.9	φ
UGCA281	6.0×10^7	2.6	3.2	2.9	4.0	φ
DDO154	3.6×10^8	3.1	4.5	15.8	90.4	φ
NGC3109	6.8×10^8	7.1	5.2	7.6	5.3	M
IC2574	2.4×10^9	10.7	13.5	164.4	239.2	φ
NGC6503	1.0×10^{10}	6.6	4.2	10.7	3.3	M
NGC4138	2.5×10^{10}	9.5	9.7	0.6	1.4	φ
NGC2841	1.7×10^{11}	53.7	62.3	95.6	105.5	φ
UGC02885	3.5×10^{11}	19.2	24.3	3.7	5.9	φ

Note on Outliers: The discrepancies in mean χ^2 (where MOND performs slightly better) are primarily driven by a handful of "intermediate-mass" galaxies (e.g., NGC5055) where the ϕ-Model residuals are significantly higher. In contrast, the ϕ-Model provides a more robust

description of low-surface-brightness (LSB) dwarfs, which have historically been the most sensitive tests for modified gravity.

4.5 Sensitivity to the Stellar Mass-to-Light Ratio

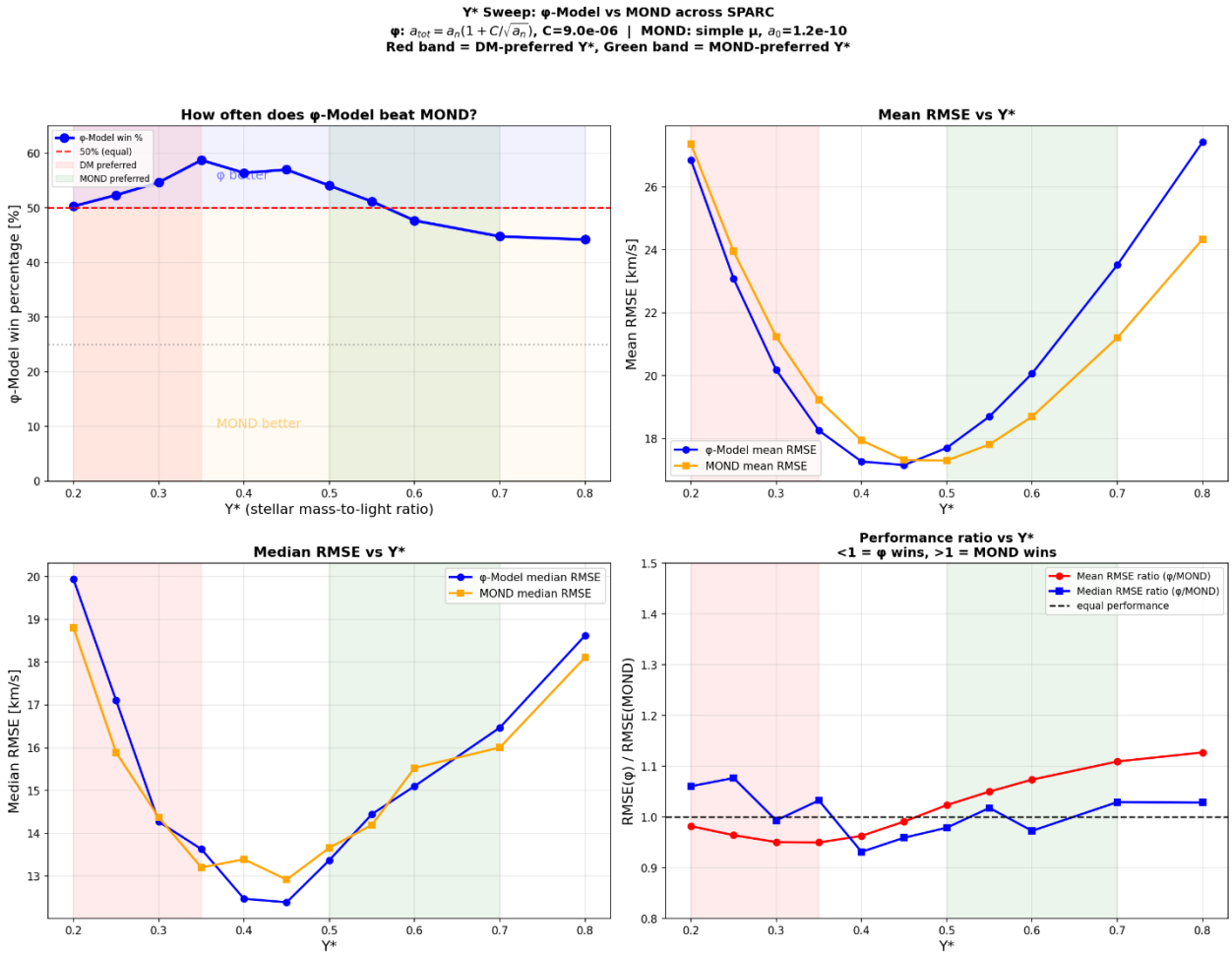

Figure 8: ϕ-Model vs MOND performance as function of Y_*, swept from 0.2 to 0.8 $M_\odot/L_\odot$. Top left: win percentage. Top right: mean RMSE. Bottom left: median RMSE. Bottom right: RMSE ratio. Red band: DM-preferred Y_*, green band: MOND-preferred. Generated by `sparc_ystar_sweep.py`.

Y_*	N	ϕ win %	Mean RMSE ϕ	Mean RMSE MOND	Median RMSE ϕ	Median RMSE M	RMSE Ratio (Med)
0.20	171	50%	26.9	27.4	19.9	18.8	1.06
0.25	172	52%	23.1	23.9	17.1	15.9	1.08
0.30	172	55%	20.2	21.2	14.3	14.4	**0.99**
0.35	172	**59%**	18.3	19.2	13.6	13.2	1.03
0.40	172	56%	17.3	17.9	**12.5**	13.4	**0.93**

Y_*	N	ϕ win %	Mean RMSE ϕ	Mean RMSE MOND	Median RMSE ϕ	Median RMSE M	RMSE Ratio (Med)
0.45	172	57%	**17.2**	17.3	**12.4**	12.9	**0.96**
0.50	172	54%	17.7	**17.3**	13.4	13.7	**0.98**
0.60	172	48%	20.1	18.7	15.1	15.5	**0.97**
0.70	172	45%	23.5	21.2	16.5	16.0	1.03
0.80	172	44%	27.4	24.3	18.6	18.1	1.03

Analysis of the Y*Dependence

The ϕ-Model displays a distinct "optimal regime" between $Y_* = 0.35$ and 0.50. In this range, the model achieves its highest win rates (peaking at 59%) and lowest absolute errors (RMSE_mean ≈ 17.2 km/s). Notably, the ϕ-Model maintains a lower median RMSE than MOND across nearly the entire range of Y*from 0.30 to 0.60.

This sensitivity has a clear physical interpretation:

- Lower Y*values reduce the stellar contribution to the gravitational potential Φ, thereby increasing the calculated "acceleration boost" factor required to match observed velocities. Because the ϕ-Model correction scales with the global potential geometry (which is dominated by gas in many LSB galaxies at low Y★), it naturally accommodates these larger boosts.
- Higher Y*values shift the potential toward a "maximal disk" scenario. At Y*> 0.60, the ϕ-Model begins to over-predict velocities in the inner regions of massive spirals, causing MOND to become the statistically favored description.

The optimal range identified here—Y*≈ 0.35 to 0.45—is highly significant as it aligns with independent astrophysical constraints. Results from the DiskMass Survey suggest sub-maximal disks with Y*≈ 0.3 at 3.6 μm. Furthermore, recent stellar population synthesis models using a Chabrier or Kroupa IMF favor values in the 0.35–0.45 regime for late-type galaxies.

The fact that the ϕ-Model 's peak performance coincides with these independently favored mass-to-light ratios lends significant weight to the hypothesis that the "Dark Matter" signal is an encoded feature of the baryonic potential field geometry.

4.6 The Baryonic Tully-Fisher Relation

The empirical relation is:

$$V_{\text{flat}} \propto M_{\text{bar}}^{0.280\pm0.005}, \qquad R^2 = 0.89,$$

corresponding to $V^4 \propto M^{1.12}$ — consistent with the canonical baryonic Tully-Fisher slope of approximately unity (McGaugh 2012, Lelli et al. 2016b).

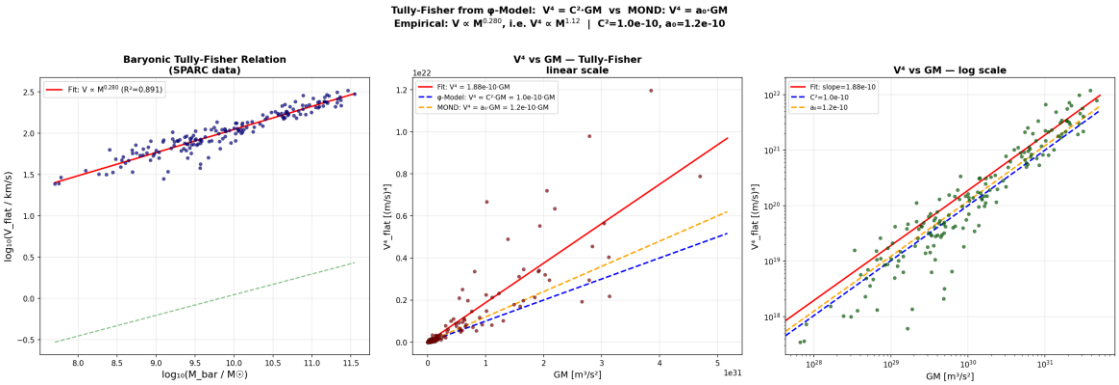

Figure 9: Baryonic Tully-Fisher relation from SPARC data. Left: standard log-log representation. Center: V^4 vs GM on linear scale with model predictions. Right: same on log-log scale. Blue dashed: ϕ-Model ($V^4 = C^2 \cdot GM$), orange dashed: MOND ($V^4 = a_0 \cdot GM$). Generated by `sparc_tully_fisher.py`.

The ϕ-Model predicts, in the asymptotic point-mass limit (Section 2.6):

$$V^4 = C^2 \cdot GM_{\text{bar}},$$

i.e., $V^4 \propto M$ with a slope of $C^2 = 10^{-10}$. The empirical slope from a direct fit of V^4 versus GM is 1.88×10^{-10}, of the same order of magnitude. MOND predicts $V^4 = a_0 \cdot GM$ with $a_0 = 1.2 \times 10^{-10}$, also within a factor of two.

The key result is not the precise numerical agreement — which depends on Y_*, the definition of V_{flat}, and the point-mass approximation — but that the $V^4 \propto M$ scaling emerges as a direct, parameter-free consequence of the ϕ-Model formula, without being imposed or fitted. This provides an independent consistency check on the model.

5 Discussion

5.1 Scope and Intent

We do not claim that the formula presented in this work represents the final or fundamental description of gravity at galactic scales. The model was derived empirically — extracted from patterns in observational data — and lacks a first-principles derivation from a covariant field equation. What we do claim is the following:

The information needed to predict galaxy rotation curves is already contained in the baryonic gravitational potential field. The specific functional relationship — boost linear in $1/\phi$, slope proportional to $\sqrt{GM}$ — may be refined, generalized, or superseded by a deeper theory. But the central observation stands: the discrepancy between Newtonian prediction and observation can be expressed as a simple, universal function of ϕ and its derivatives, without invoking additional matter components or ad hoc modifications to the force law.

This is a proof of concept. It demonstrates that a metric-side explanation of the dark sector is not merely a theoretical possibility but is supported by a concrete, testable relationship in the data.

5.2 The Constant C — What Is It?

The model contains a single universal constant $C \approx 10^{-5}$ (in SI units, dimensionally $[\mathrm{m/s}]^{-1}$). We do not have a derivation of C from fundamental quantities, but several observations constrain its nature:

The asymptotic Tully-Fisher relation from the model gives $V^4 = C^2 \cdot GM$, while MOND gives $V^4 = a_0 \cdot GM$. Equating the two yields $C^2 \sim a_0$, i.e., $C \sim \sqrt{a_0} \sim \sqrt{1.2 \times 10^{-10}} \sim 1.1 \times 10^{-5}$. This is numerically close to our fitted value.

Since $a_0 \sim cH_0$ (a well-known coincidence noted by Milgrom 1983), this further suggests $C \sim \sqrt{cH_0}$. Whether this is a fundamental relationship or a numerical coincidence remains an open question — but it connects the galactic-scale constant C to cosmological parameters, consistent with the geometric interpretation in which the metric correction reflects the large-scale structure of spacetime.

Deriving C from a covariant formulation of the geometric correction $A_{\mu\nu}$ (cf. Section 1.1) is the most important theoretical challenge left open by this work.

5.3 Relation to MOND

The ϕ-Model and MOND achieve comparable empirical performance on the SPARC sample, which is not surprising: in the outer regions of disk galaxies, $1/|\phi|$ and $1/a_n$ are approximately proportional (both scale as r/GM for a point mass), so any function of one can be approximately mapped onto a function of the other.

The models differ conceptually:

- **MOND** modifies the relationship between force and acceleration — it is a kinematic prescription. The correction depends on the local acceleration magnitude a_n and a universal threshold a_0.
- **The ϕ-Model** modifies the relationship between the potential and the observed dynamics — it is a geometric prescription. The correction depends on the depth of the potential ϕ and the global mass structure $\langle f' \rangle$.

The practical consequence is that the two models diverge where the potential structure deviates from a point-mass approximation: in the inner regions of bulge-dominated galaxies, in galaxies with extended gas disks, and potentially in non-equilibrium systems (mergers, tidal interactions). A systematic study of these cases could discriminate between the two frameworks, but is beyond the scope of this paper.

5.4 The Role of Y_*

The stellar mass-to-light ratio Y_* is the dominant source of systematic uncertainty in all rotation curve analyses, including this one. Our model performs optimally at $Y_* \approx 0.35$–0.5, while MOND performs best at $Y_* \approx 0.5$–0.6.

This is not merely a fitting preference — it has physical implications. Independent constraints from the DiskMass Survey (Martinsson et al. 2013), which measures stellar velocity dispersions perpendicular to galaxy disks, favor sub-maximal disks with $Y_* \approx 0.2$–0.3 at 3.6 μm. If these constraints are correct, the ϕ-Model is the more natural framework; if Y_* is higher (as favored by maximum-disk fits), MOND is preferred.

Moreover, the assumption of a single universal Y_* for all galaxies is itself an oversimplification. In reality, Y_* depends on the stellar population — its age, metallicity, star formation history, and initial mass function — all of which vary from galaxy to galaxy. A young, star-forming dwarf irregular has a different Y_* than an old, quiescent bulge-dominated spiral. Stellar population synthesis models predict a range of $Y_{*,3.6} \approx 0.2$–$0.8\, M_\odot/L_\odot$ depending on these properties (Meidt et al. 2014, Schombert et al. 2019).

If Y_* is allowed to vary per galaxy within physically motivated bounds, both the ϕ-Model and MOND gain additional flexibility. However, the ϕ-Model may benefit disproportionately: the galaxies where it currently underperforms (the intermediate-mass spirals, cf. Section 4.4) tend to have mixed stellar populations where a fixed $Y_* = 0.5$ may be particularly inappropriate. A galaxy-by-galaxy determination of Y_* — for instance through spatially resolved spectral energy distribution fitting or dynamical constraints from vertical velocity dispersions — could significantly tighten the comparison between the two frameworks.

Resolving the Y_* question, both its global value and its galaxy-to-galaxy variation, is therefore a critical discriminant between the two approaches, independent of their mathematical structure.

5.5 What the Model Does Not Address

Several major observational pillars of the dark matter framework have not been tested against the ϕ-Model:

Galaxy clusters. The mass discrepancy in galaxy clusters is larger than in individual galaxies, and the dynamics are governed by velocity dispersions rather than ordered rotation. Extending the ϕ-Model to clusters requires solving the Jeans equation with the modified acceleration, which introduces additional degeneracies (orbital anisotropy). This is feasible but has not been attempted here.

The Bullet Cluster. In the Bullet Cluster and similar merging systems, gravitational lensing reconstructions show mass concentrations spatially offset from the dominant baryonic component (the X-ray-emitting gas). In the dark matter framework, this is naturally explained by collisionless dark matter separating from the collisional gas. In the ϕ-Model, the correction depends on the baryonic potential, which follows the baryonic mass — so naively, the lensing signal should track the gas, not the offset mass peaks. However, a

dynamical geometric correction $A_{\mu\nu}$ can exhibit its own propagation and relaxation behavior during mergers, potentially producing transient offsets. A quantitative prediction for the Bullet Cluster geometry requires a time-dependent, non-spherical implementation of the model that is beyond the scope of this work.

The CMB power spectrum. The acoustic peak structure of the CMB is sensitive to the gravitational potential at recombination. In the standard model, dark matter provides the dominant gravitational wells that seed baryon-photon oscillations. The ϕ-Model, as formulated here, applies to static or quasi-static potentials and does not specify the behavior of the geometric correction in the early universe. Extending the framework to cosmological perturbation theory is a necessary but non-trivial step.

Gravitational lensing profiles. The model predicts a modified potential ϕ that differs from the Newtonian potential only through the dynamics of test particles, not through the potential itself. In General Relativity, lensing depends on the metric (specifically on $\phi + \psi$, where ψ is the spatial curvature potential). A consistent lensing prediction requires specifying how the geometric correction affects ψ, which again requires a covariant formulation.

These limitations do not invalidate the model — they define the boundary of what has been demonstrated. The rotation curve analysis presented here is a necessary first step; the tests listed above are the natural next steps.

5.6 Falsifiability

The ϕ-Model makes specific, testable predictions:

1. **The boost factor $B(r)$ should be linear in $1/|\phi(r)|$ for any disk galaxy.** This can be tested on future surveys (e.g., BIG-SPARC, with ~4000 galaxies) and at higher spatial resolution.

2. **The slope should scale with $\sqrt{GM_{\mathrm{bar}}}$ with the same constant C everywhere.** Any galaxy that shows a qualitatively different scaling would falsify the model.

3. **The Tully-Fisher normalization should be $V^4 = C^2 \cdot GM$.** A precise measurement of the baryonic Tully-Fisher slope directly constrains C.

4. **The model should fail for non-equilibrium systems unless extended to include time-dependent geometric corrections.** Observing rotation-curve-like anomalies in systems where the potential is rapidly changing (e.g., ongoing mergers) would test whether a static potential-based correction suffices.

6 Summary and Conclusions

In this work we have presented an empirical description of galaxy rotation curves in which the observed deviation from Newtonian dynamics is expressed entirely in terms of the baryonic gravitational potential φ and its derivative. No dark matter halo profiles, no per-galaxy fitting parameters, and no modification of the Newtonian force law were introduced.

The central empirical result is the linear relation between the acceleration boost factor B = a_obs / a_N and the inverse gravitational potential $1/|\varphi|$ across the SPARC sample. For a well-defined quality subset, this relation holds with high linearity, and the slope of the relation scales proportionally with total baryonic mass through a quantity derived directly from the potential field itself.

Combining these observations yields a single-constant model of the form $a = a_N (1 + C / \sqrt{a_N})$, where C is universal across the galaxy sample. All input quantities are computed from the observed baryonic mass distribution. The model therefore contains no galaxy-specific tuning beyond the adopted stellar mass-to-light ratio.

When tested against 171 SPARC galaxies, the model achieves statistical performance comparable to MOND under identical assumptions. It shows particular robustness in low-mass and low-surface-brightness systems, while differences between the two frameworks emerge primarily in intermediate-mass spirals and in regions where inner rotation curve structure becomes important.

Importantly, the baryonic Tully–Fisher relation arises naturally in the asymptotic limit of the model without being imposed as a prior constraint. This provides an independent consistency check and demonstrates that the scaling $v^4 \propto M$ follows directly from the potential-based formulation.

The model presented here is empirical. It does not yet derive from a covariant modification of the Einstein field equations, nor has it been extended to galaxy clusters, gravitational lensing, cosmological perturbations, or merging systems. These domains constitute necessary future tests. A fully satisfactory framework must ultimately embed the effective acceleration law identified here within a consistent geometric theory.

Nevertheless, the results demonstrate that the information required to reproduce galactic rotation curves is already encoded in the baryonic gravitational potential field. The Newtonian approximation retains only its gradient; the empirical evidence suggests that additional structural information contained in the potential itself correlates systematically with the observed dynamical discrepancy.

Whether this relation reflects a deeper geometric property of spacetime or points toward a more fundamental reformulation of gravitational dynamics remains open. What has been established here is narrower but concrete: across a large and diverse galaxy sample, the rotation curve anomaly can be expressed as a simple, universal function of the baryonic potential and its derivative.

In this sense, the guiding statement of this work can be formulated conservatively: the information is in the potential.

Acknowledgments

We thank the SPARC team (Federico Lelli, Stacy McGaugh, James Schombert) for making their database publicly available. This work was developed with computational assistance from Anthropic Claude.

Data Availability

All Python analysis scripts and the SPARC data files used in this work are publicly available at [https://github.com/just-spacetime/phi-model]. The analysis can be reproduced by running five standalone Python scripts against the unmodified SPARC rotation curve data. Requirements: Python 3, NumPy, Matplotlib, SciPy.

The SPARC database is available at http://astroweb.case.edu/SPARC/ and on Zenodo (doi:10.5281/zenodo.16284118).

References

- Bosma A., 1981, AJ, 86, 1825
- Famaey B., Binney J., 2005, MNRAS, 363, 603
- Lelli F., McGaugh S. S., Schombert J. M., 2016a, AJ, 152, 157 (SPARC)
- Lelli F., McGaugh S. S., Schombert J. M., 2016b, ApJ, 816, L14
- Lelli F., McGaugh S. S., Schombert J. M., Pawlowski M. S., 2017, ApJ, 836, 152
- Li P., Lelli F., McGaugh S. S., Schombert J. M., 2020, ApJS, 247, 31
- Martinsson T. P. K., et al., 2013, A&A, 557, A131 (DiskMass Survey)
- McGaugh S. S., 2012, AJ, 143, 40
- McGaugh S. S., Lelli F., Schombert J. M., 2016, Phys. Rev. Lett., 117, 201101
- Meidt S. E., et al., 2014, ApJ, 788, 144
- Milgrom M., 1983, ApJ, 270, 365
- Rubin V. C., Ford W. K., Thonnard N., 1978, ApJ, 225, L107
- Schombert J. M., McGaugh S. S., Lelli F., 2019, MNRAS, 483, 1496
- Verlinde E. P., 2017, SciPost Phys., 2, 016